This article has been accepted for publication in a future issue of this journal, but has not been fully edited. Content may change prior to final publication.
DOI: 10.17775/CSEEJPES.2025.02610

Multi-Degree-of-Freedom Control Framework for HVDC Transmission Converters[1]

Haobo Zhang, Jinyu Wen, *Senior Member, IEEE*, *Fellow*, *CSEE*, Wang Xiang, *Senior Member, IEEE*, Weixing Lin, *Member, IEEE*, Meng Zhou, Wenping Zuo, Shijie Cheng, *Life Fellow, IEEE*

***Abstract*—This paper systematically investigates the multi-degree-of-freedom (Multi-DoF) control framework of high voltage direct current (HVDC) converters based on their topological characteristics and control requirements. First, this study reveals that the control degrees of freedom (CDoF) of a converter are determined by its topology. Specifically, a line-commutated converter (LCC) possesses only one CDoF, a voltage source converter (VSC) has two, and a modular multilevel converter (MMC) can theoretically achieve up to eight. However, only six CDoF are practically necessary for MMC. Despite this, existing MMC control strategies utilize only four CDoF, limiting control flexibility. To overcome this issue, this paper proposes a six-degree-of-freedom (6 DoF) control framework for MMC, which enables asymmetric and precise regulation of DC voltage and SM capacitor voltage compared to the existing MMC control. Based on this framework, corresponding control strategies are designed for MMCs in HVDC systems with different control objectives. Finally, a two-terminal MMC-HVDC system is built on the PSCAD/EMTDC to verify the effectiveness of the proposed 6 DoF control.**

***Index Terms*—DC transmission, line commutated converter, voltage source converter, modular multilevel converter, control degree of freedom.**

I. Introduction

Modern high-voltage direct current (HVDC) transmission technology began to develop in the mid-20th century and has advanced rapidly. It has evolved into two main types: conventional HVDC transmission and flexible HVDC transmission, both of which have been widely applied in large-scale projects. Conventional HVDC transmission uses thyristor-based line commutated converter (LCC). LCC offers advantages such as low cost and strong resistance to transient disturbances. However, they lack self-commutation capability and rely on the AC grid for commutation. In addition, the risk of commutation failure remains a major threat to grid security.

In contrast, flexible HVDC transmission uses fully controllable insulated gate bipolar transistor (IGBT) devices. The main topologies include voltage source converters (VSC) and modular multilevel converter (MMC). These converters offer self-commutation, decoupled active and reactive power control, and the ability to connect to passive networks.

LCC uses thyristors, which can only be turned on but not actively turned off. By adjusting the firing time of the thyristors, LCC regulates the DC voltage and controls active power. Therefore, its control method is primarily based on firing angle regulation [1]. For instance, many studies have proposed improved control strategies to prevent commutation failures under grid faults [2]-[9]. Further research has introduced frequency control and damping control to support the AC grid during steady-state operation [10]-[16].

VSC uses IGBTs, which can be both turned on and turned off. This gives VSC greater flexibility than LCC. The existing control strategies of VSC can be classified into indirect current control [17]-[19] and direct current control [20]. Most practical VSCs use direct current control in the synchronous rotating reference frame (dq-reference frame), also known as vector current control. To improve stability performance in weak AC grids, researchers have developed grid-forming control strategies that do not rely on phase-locked loops (PLL) [21]-[44]. These strategies allow VSCs to establish voltage amplitude and frequency independently, ensuring fast response to grid fluctuations while providing voltage and frequency support.

MMC has a modular topology that allows independent modulation of the upper and lower bridge arms. Traditional MMC control strategies are similar to those of VSCs. The main objectives are active/reactive power control, DC voltage control, and grid-forming control. Therefore, most MMC control systems use a vector current control structure, similar to VSCs. However, different from VSC, the modulation of sub-module (SM) capacitors in MMC generates second harmonic circulating currents, which require additional circulating current suppression control [20].

With the increasing demand for long-distance DC power transmission, current limiting under DC faults has become a major challenge for the MMC that is only based on the vector current control. To reduce the requirements for DC circuit breakers and improve fault ride-through capability, researchers have modified the conventional vector control structure. By introducing a DC current control loop, they enable direct regulation of the DC voltage, allowing MMC to limit the fault current to continue operating during DC faults [45]-[49].

With the large-scale integration of renewable energy and power electronics-based devices into AC grids, the strength and inertia of power systems are gradually decreasing. MMCs contain hundreds or thousands of SM capacitors, which can act

This work was supported in part by the National Key Research and Development Program of China (No. 2022YFB2405400) and in part by the National Natural Science Foundation of China (No. 52237004). (Corresponding author: *Jinyu Wen*).

Haobo Zhang, Jinyu Wen, Wang Xiang, Weixing Lin, and Shijie Cheng are with the State Key Laboratory of Advanced Electromagnetic Technology, Huazhong University of Science and Technology, 430074, Wuhan, China (e-mail: zhanghaobo9902@foxmail.com; jinyu.wen@hust.edu.cn; xiangwang 1003@hust.edu.cn; weixinglin@foxmail.com; sjcheng@hust.edu.cn).

Meng Zhou and Wenping Zuo are with Gridmind Technology (Wuhan) Co., Ltd, Wuhan 430073, China (zhoumeng4077@foxmail.com; radio.zuo@ foxmail.com).

as energy storage devices and actively support grid stability. Early studies proposed differential-mode and common-mode control of MMC capacitor energy to balance arm and phase energy separately [50]. However, these strategies relied on indirect current control and lacked fault current limiting capability. Later research addressed these limitations by adding differential-mode and common-mode energy control into vector current control [51][52]. Nevertheless, capacitor energy must be regulated to maintain its rated value, ensuring stable operation. Referring to the control strategies of hybrid MMCs, reference [53] proposed a capacitor energy control method based on a DC current controller. This approach introduced variable nearest level modulation (NLM), allowing MMC to manage capacitor energy flexibly. Building on this control framework, many studies have explored MMC capacitor energy-based support strategies, including AC fault ride-through [54][55], frequency/inertia support [56][58], and weak AC grid integration [59]-[61].

The above analysis shows that HVDC converter topologies and control strategies continue to evolve to meet the needs of new power systems. However, most research focuses on improving control functions and applications, while the relationships between different control strategies and the evolution of control structures remain insufficiently explored.

To address this gap, The main novelty and contributions of this paper are listed:

- A new perspective from control degree of freedom (CDoF) is presented to propose the viewpoint that converter topology determines its control flexibility. On this basis, multi-degree-of-freedom (Multi DoF) control framework is developed to evaluate the control capability of different HVDC converters, systematically identifying their inherent limitations and guiding control architecture evolution.
- A novel 6 DoF control strategy for MMCs is developed, which extends traditional control methods by enabling asymmetric regulation of arm DC voltages and submodule capacitor voltages. This added flexibility significantly improves the operational reliability MMC-HVDC, especially under DC faults.

The paper is organized as follows. Sections II, III, and IV analyze the control requirements, objectives and schemes of LCC, VSC, and MMC, respectively. Section V introduces the CDoF-based classification, summarizes the existing limitations of MMCs, and proposes the 6 DoF control strategy. Section VI validates its enhanced flexibility through simulation. Section VII discusses the CDoF requirements for grid-forming MMCs in future power systems. Conclusions are drawn in Section VIII.

II. Line Commutated Converter

A. Control Requirements of LCC

Fig. 1 illustrates the topology of an LCC converter. In Fig. 1, X_T represents the equivalent commutation reactance, v_s is the voltage of the AC grid, and V_{dcp} and V_{dcn} denote the positive and negative-pole DC-side voltages, respectively. Since thyristors can only be actively turned on but not turned off, the AC side must provide a stable AC voltage to maintain a stable DC-side voltage.

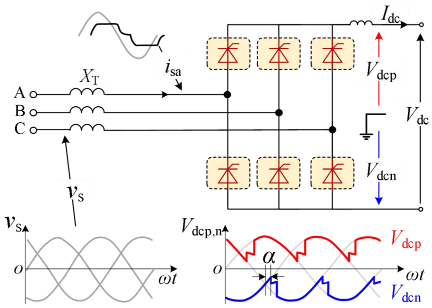

Fig. 1 Topology diagram of LCC.

During normal operation, when the LCC triggers the thyristors, the DC-side voltage waveforms can be modulated based on the circuit topology, as shown in the red and blue curves in Fig. 1. It is evident that different triggering times result in different DC-side voltage. Therefore, the LCC can adjust the firing angle α to control the turn-on timing of the thyristors, thereby regulating the DC voltage. The relationship between the firing angle and the DC voltage is given by:

$$\begin{cases} V_{dc} = 1.35 V_{ac} \cos\alpha_r - \dfrac{3}{\pi} X_T I_{dc} \text{ , Rectifier} \\ V_{dc} = 1.35 V_{ac} \cos\alpha_i + \dfrac{3}{\pi} X_T I_{dc} \text{ , Inverter} \end{cases} \tag{1}$$

where V_{ac} is the RMS value of the line voltage on the valve side of the transformer.

From the above analysis, it is evident that due to the semi-controlled characteristic of thyristors, LCC has only one control variable, which is the firing angle α. During normal operation, the LCC's control system must determine the appropriate firing angle based on the given control objectives.

To quantify the control flexibility of converter, the concept of CDoF is proposed in [60], which characterizes the number of control variables and serves as an indicator to measure the control ability. Thus, according to the definition of CDoF, LCC has one CDoF.

B. Existing Control of LCC

To determine the firing angle α, the typical control structure of rectifier and inverter stations in LCC-HVDC system is shown in Fig. 2. The detailed definition of the variables in Fig. 2 can be found in reference [62]. On the rectifier side, the control strategy adopts constant DC current control. While on the inverter side, the control strategy includes constant DC current control and constant extinction angle (γ) control. Additionally, the inverter side is equipped with a Voltage-Dependent Current Order Limiter (VDCOL). The VDCOL control adjusts the DC current reference (I_{dref}) based on the DC voltage. During AC transient faults, it dynamically manages reactive power consumption, helping to reduce AC overvoltage [63][64].

To prevent instability caused by simultaneous operation of current controllers at both terminals, the reference value of the inverter-side current regulator is typically set at 0.1p.u., lower than that of the rectifier-side (current margin I_{margin}). This method, known as the "current margin method", was first applied in the 1954 Gotland HVDC project in Sweden.

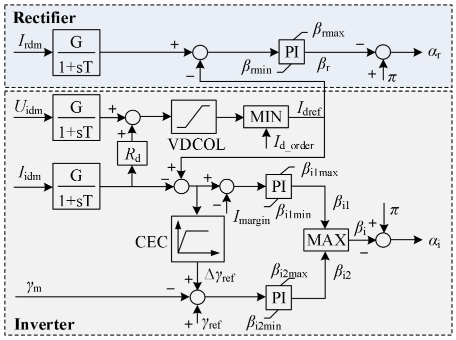

Fig. 2 Control of LCC at the rectifier and inverter stations.

Since LCC relies on the external AC grid to provide commutation voltage, faults in the receiving-end AC system or switching operations near the inverter station can lead to voltage dips, making commutation failure highly likely [65]-[67]. Commutation failure can temporarily interrupt the HVDC link, causing a large power disturbance in the power system. One of the common methods to mitigate commutation failure is to improve control strategies. Despite various improved control strategies being developed in [1]-[9], all of these are implemented by regulating the firing angle.

Beyond commutation failure mitigation, efforts have also been made to enhance the grid support capabilities of LCC-HVDC systems. Some system-level control functions, such as frequency control [10]-[13] and damping control [14]-[16], were also designed by adding outer-loop controllers to the basic control shown in Fig. 2. Although the control structures of these schemes are quite complex, the ultimate control variable remains the firing angle.

In summary, due to the inherent thyristor-based characteristics, the CDoF of LCC is constrained to regulating the firing angle. Hence, all the control strategies of the LCC can be referred to as 1 DoF control.

III. Voltage Source Converter

A. Control Requirements of VSC

In 1990, Boon-Teck Ooi and his team at McGill University in Canada first proposed the concept of VSC [17]-[19]. Take the two-level VSC (TL-VSC) as an example, the topology is shown in Fig. 3. As can be seen, VSC replaces the thyristors in Fig. 1 with fully controllable IGBTs. Consequently, the VSC does not require commutation voltage from the AC side. By controlling the switching actions (turning on and off) of the IGBTs, VSC can generate an AC voltage wave automatically.

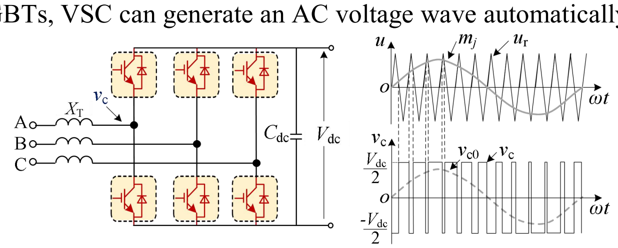

Fig. 3 Topology diagram of TL-VSC.

When the VSC operates, the control system should first determine the desired AC voltage waveform to be output at the AC side, i.e., m_j in Fig. 3 (per unit value, j = a, b, c). Further, the pulse width modulation (PWM) method is employed to use m_j as the modulation wave and compare m_j with the triangular carrier wave u_r to generate the trigger pulses required for the IGBT. By applying the turn-on and turn-off signals to the IGBTs multiple times within one power frequency cycle, a pulse wave v_c with two levels ($V_{dc}/2$ and $-V_{dc}/2$) is produced on the AC side. According to the impulse equivalence principle, v_c can be equivalently represented as the fundamental frequency voltage v_{c0}. Here, v_{c0} shares the same characteristics as the m_j.

Taking phase a as an example, m_j can be expressed as:

$$m_a = M_{ac}\cos(\omega_0 t - \varphi_{ac}) \tag{2}$$

where, M_{ac} and φ_{ac} are the amplitude and phase of the voltage modulation wave m_j, respectively. Hence, the relationship between v_{c0} and m_j satisfies:

$$v_{c0\_a} = \frac{1}{2} m_a V_{dc} = \underbrace{0.5 M_a V_{dc}}_{V_{ac}} \cos(\omega_0 t - \varphi_{ac}) \tag{3}$$

where V_{ac} is the amplitude of the AC side voltage of the VSC.

From the above analysis, it can be concluded that the control objective of the VSC is to determine the required AC voltage modulation wave m_j, including 2 control variables: the voltage amplitude M_{ac} and phase φ_{ac}. Therefore, the CDoF of the VSC can be increased to 2 compared to LCC.

B. Existing Control of LCC

1) Indirect current control

To determine the AC voltage modulation wave m_j, references [17]-[19] present the basic control structure of VSCs, as shown in Fig. 4. In this control framework, the VSC directly sets the amplitude V_{ac} and phase φ_{ac} of the AC modulation voltage. Using a three-phase sine wave generator, VSC can then generate the required voltage modulation waves m_j.

To regulate power, power control loops are applied at the outer loop of the control architecture shown in Fig. 4. Based on the mathematical model of VSC, control of active power P_{ac} and DC voltage V_{dc} can be achieved by directly adjusting the phase angle φ_{ac} of the AC voltage. Meanwhile, reactive power Q_{ac} and AC voltage V_m can be regulated by directly controlling the amplitude V_{ac} of the AC voltage.

During normal operation, the VSC dynamically calculates the required output voltage amplitude V_{ac} and phase φ_{ac} based on the deviation between the actual and reference values of active and reactive power. This indirectly adjusts the output current of the VSC, thereby achieving power regulation. Due to this indirect relationship, this control method is referred to as indirect current control. However, it has certain drawbacks, including slower current response, high dependence on system parameters, and increased risk of VSC valve overcurrent during external grid disturbances [68].

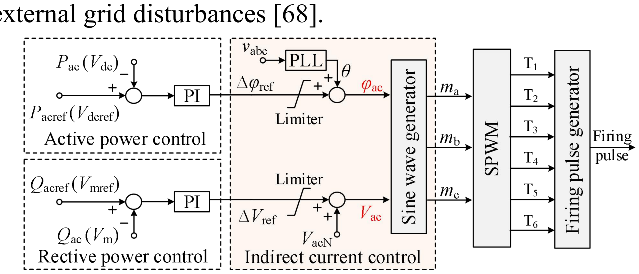

Fig. 4 Indirect current control of VSC.

2) *Direct current control*

To achieve fast control of the AC output current of the converter and ensure fault current limiting, the control architecture of VSC has gradually evolved into a direct current control. There are three implementation methods, each corresponding to a different reference frame (abc, αβ, and dq-reference frame). Among them, the vector current control method, which is based on the dq-reference frame combined with PI controllers, is the most practical, as shown in Fig. 5.

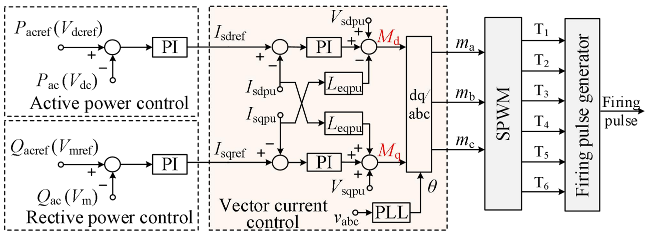

Fig. 5 Vector current control of VSC.

Unlike indirect current control shown in Fig. 4, the voltage modulation wave m_j in vector current control is not generated by the sine wave generator, but is obtained through the inverse Park transformation from the dq-axis modulation signals (M_d and M_q). The relationship between M_d, M_q, and m_j is given by the following equation:

$$m_a = \underbrace{\sqrt{M_d^2 + M_q^2}}_{V_{ac}} \cos(\omega_0 t - \underbrace{(\theta + \arctan(M_q / M_d))}_{\varphi_{ac}}) \quad (4)$$

As can be seen, the amplitude V_{ac} of the AC modulation voltage is adjusted by modifying the size of dq-axis modulation signals (M_d and M_q). Additionally, since the reference phase θ for the inverse Park transformation is determined by the PLL based on the measured grid voltage, the phase φ_{ac} of the AC modulation voltage can be controlled by adjusting the ratio between M_d and M_q. Thus, the modulation signals (M_d and M_q) are equivalent to these (V_{ac} and φ_{ac}) in Fig. 4.

To obtain the modulation signals M_d and M_q for fast AC current regulation, the vector current control introduces a decoupling control branch. This allows independent control of active and reactive power, as illustrated by the gain L_{eqpu} in Fig. 5. Under this control framework, active power control and reactive power control are achieved through d-axis and q-axis current control, respectively.

3) *AC grid-forming control*

With the increasing integration of power electronic devices and renewable energy sources into AC grids, power systems are gradually exhibiting low short-circuit ratio (SCR) characteristics. The PLL-based vector current control strategy (also known as grid-following control, as shown in Fig. 5) faces stability risks due to parameter sensitivity and lack of grid support capability. To address this issue, references [21]-[44] proposed grid-forming control strategies for VSC that do not rely on PLL. These grid-forming control schemes autonomously establish AC voltage amplitude and frequency, enabling instantaneous response to grid dynamics and providing voltage and frequency support. The basic framework of grid-forming control can be summarized in Fig. 6.

In Fig. 6, grid-forming control consists of an autonomous synchronization loop and a voltage control loop. The autonomous synchronization loop determines the phase of the converter output voltage, thus regulating the output frequency. It can be implemented using various methods, including: 1. Power synchronization control [23]-[31]. 2. Matching control [32]-[35]. 3. Virtual oscillator control [36]-[44].

Power synchronization control mimics the power characteristics of synchronous generators (SGs) by replicating the SG's rotor motion equation and excitation control. This allows autonomous regulation of AC voltage amplitude and frequency. However, this method requires a stable DC source, making it unsuitable for constant DC voltage stations.

To address this limitation, researchers have developed matching control, which draws an analogy between the DC capacitor of the converter and the dynamics of an SG's rotor, allowing regulation of DC-side voltage.

Virtual oscillator control models the converter as a weakly nonlinear oscillator, enabling it to autonomously generate sinusoidal voltage amplitude and frequency [69]. This method enhances synchronization stability among multiple converters.

In terms of the voltage control loop, there are two main structures: dual-loop voltage control and single-loop voltage control. Reference [21] suggests that when the AC-side reactance is large, single-loop voltage control provides better dynamic performance and stability. However, when the AC reactance is not very large, these advantages become less significant. Additionally, since single-loop voltage control lacks a current regulation loop, dual-loop voltage control is more effective in limiting current during AC faults [69]. However, the presence of current control may prevent the converter from fully exhibiting voltage source characteristics during grid disturbances. Regardless of the voltage control method used, the implementation of voltage regulation still follows either the indirect current control framework (in Fig. 4) or the vector current control framework (in Fig. 5).

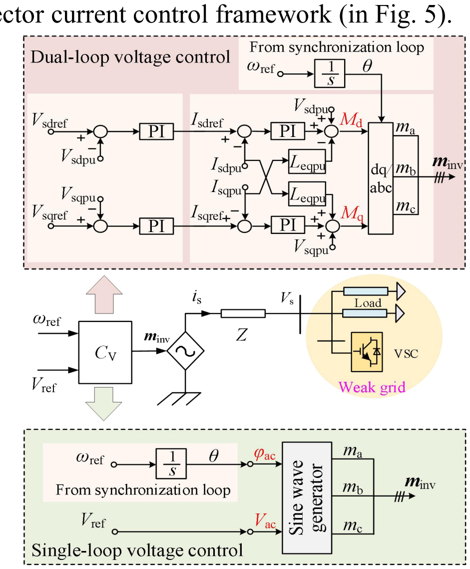

Fig. 6 AC grid-forming control of VSC.

Based on the analysis, the existing control structures for VSC mainly include indirect current control, vector current control, and AC grid-forming control. The control principle of these methods relies on determining two key parameters of the VSC AC voltage: its amplitude V_{ac} and phase φ_{ac}. Therefore, these control structures can all be referred to as 2 DoF control.

IV. Modular Multilevel Converter

A. Control Requirements of MMC

Unlike the VSC converter, which uses centralized IGBT in its arms, the MMC converter adopts a modular design, as shown in Fig. 7 (a). Each SM consists of at least two IGBTs, allowing MMC to insert and bypass SMs. Additionally, the upper and lower arms of an MMC can be modulated separately, providing greater control flexibility than VSC.

Taking a single-phase as an example, the single-phase equivalent circuit of MMC is illustrated in Fig. 7 (b). To simplify theoretical analysis, the leakage reactance X_T of the coupling transformer, as well as the resistance and inductance of the MMC arms, are neglected in Fig. 7.

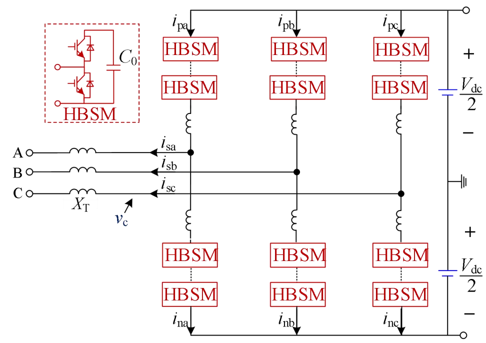

(a) Topology of MMC

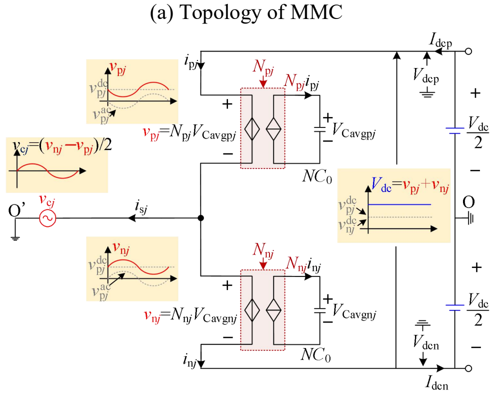

(b) Single-phase equivalent circuit of MMC

Fig. 7 Operational schematic diagram of MMC.

The operating principle of MMC can be summarized as follows: During normal operation, the MMC should first determine the desired modulation voltage waveforms for the upper and lower arms (v_{pj} and v_{nj}) based on the control objectives. Then, the NLM method is applied to calculate the number (N_{pj} and N_{nj}) of SMs required to be inserted in each arm. The controller selects the appropriate SMs and applies trigger pulses, thereby generating the AC-side voltage v_{cj} and DC voltage V_{dc} through modulation on both the AC and DC sides. The relationship between the arm modulation voltage and the AC/DC-side voltages can be approximately expressed as:

$$\begin{cases} v_{cj} = \dfrac{v_{nj} - v_{pj}}{2} \\ V_{dc} = v_{nj} + v_{pj} \end{cases} \tag{5}$$

Therefore, the core of MMC control lies in determining the arm modulation voltage. Since MMC primarily converts between the fundamental-frequency AC voltage and DC voltage, the arm modulation voltage in (5) can be further decomposed into fundamental-frequency AC components (v_{pj}^{ac} and v_{nj}^{ac}) and DC components (v_{pj}^{dc} and v_{nj}^{dc}). Additionally, as shown in Fig. 7 (b), the arm modulation voltages are also influenced by the average SM capacitor voltage (V_{Cavgpj} and V_{Cavgnj}) and the number of inserted SMs (N_{pj} and N_{nj}), satisfying the following relationship:

$$\begin{cases} v_{pj} = N_{pj} V_{Cavgpj} \\ v_{nj} = N_{nj} V_{Cavgnj} \end{cases} \tag{6}$$

In summary, topological characteristics of MMC determine that its control system must have the ability to determine the following six electrical quantities (eight control variables): The amplitude (V_{acp}, V_{acn}) and phase (φ_{acp}, φ_{acn}) of v_{pj}^{ac} and v_{nj}^{ac}; The amplitude of v_{pj}^{dc} and v_{nj}^{dc}; The SM capacitor voltages V_{Cavgpj} and V_{Cavgnj}. Thus, MMC has eight CDoF theoretically.

B. Existing Control of MMC

Based on the above analysis, although MMC arms can be modulated separately, existing MMC-HVDC projects adopt a symmetric modulation method. Under this condition, the AC and DC components of the upper and lower arm modulation voltages are identical, where the AC components are equal in magnitude but opposite in sign ($v_{nj}^{ac} = -v_{pj}^{ac}$), the DC components are equal ($v_{pj}^{dc} = v_{nj}^{dc}$), and the SM capacitor voltages are also equal (V_{Cavgpj}=V_{Cavgnj}). Therefore, MMC's control only needs to determine the following three electrical quantities (four control variables): The amplitude (V_{acp}, V_{acn}) and phase (φ_{acp}, φ_{acn}) of v_{pj}^{ac} or v_{nj}^{ac}; The amplitude of v_{pj}^{dc} or v_{nj}^{dc}; The SM capacitor voltages V_{Cavgpj} or V_{Cavgnj}.

1) 2-Degree-of-Freedom Control

Fig. 8 illustrates the mainstream MMC control structure. The key difference between MMC control and VSC control lies in the arm voltage calculation and NLM.

To determine the AC component of the arm modulation voltage (v_{pj}^{ac} or v_{nj}^{ac}), the control must determine both its amplitude and phase. This control objective is identical to the generation of modulation wave m_j in VSC, as discussed in Section III.B. Therefore, MMC can adopt the same 2 DOF control as VSC, including indirect current control, vector current control, and AC grid-forming control. Fig. 8 illustrates the vector current control, in which the amplitude and phase of m_j are determined by adjusting M_d and M_q.

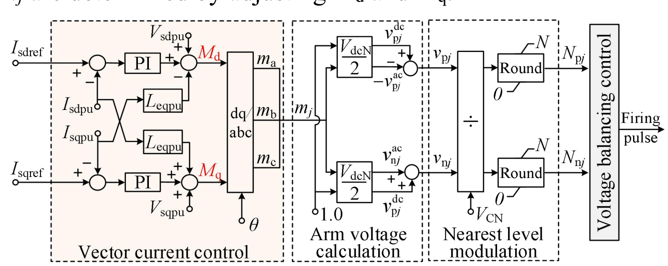

Fig. 8 2-degree-of-freedom-control of MMC.

To determine the DC component (v_{pj}^{dc} or v_{nj}^{dc}), existing MMC control methods typically assume a constant DC voltage. As a result, the DC component of the arm voltage is fixed at 1.0

p.u. in Fig. 8. Although this assumption does not affect the steady-state operation of MMC, it makes flexible DC voltage regulation more challenging. It should be noted that while the control method illustrated in Fig. 8 enables DC voltage regulation, it is achieved by regulating the AC components of the arm modulation voltage (M_d and M_q in Fig. 8) to control AC power and finally control DC voltage. Thus, this approach will cause a control coupling between DC voltage and AC voltage.

Additionally, according to the NLM principle, the number of inserted SMs must be calculated. To simplify control, it often assumes that the average SM capacitor voltages (V_{Cavgpj} and V_{Cavgnj}) are constant at the rated value V_{CN}. Therefore, in Fig. 8, NLM typically uses V_{CN} as the denominator. However, to ensure the accuracy of the SM insertion count, this will prevent MMC from regulating the SM capacitor voltage.

In summary, although MMC offers greater topological flexibility, the control strategy shown in Fig. 8 only has two control variables, M_d and M_q, which allow regulation of the AC voltage amplitude and phase but not the DC voltage or SM capacitor voltage. Therefore, this control approach is also referred to as MMC's 2 DoF control.

Based on this 2 DOF control framework, studies [70]-[72] introduced third-harmonic voltage injection in the arm voltage calculation of Fig. 8, improving the power transfer capacity and DC voltage utilization. To balance SM capacitor voltages between phases and arms, studies [50]-[52] proposed an MMC energy balancing control framework. Further considering AC system support, various enhanced control strategies were developed for MMCs, all based on the vector current control. These strategies include frequency and inertia support control [73]-[76], voltage support control [77]-[80], and damping support control [81]-[87].

Although third-harmonic injection control, energy balancing control, and grid support control serve as enhancements to the control shown in Fig. 8, their basic principle remains the same: achieving control objectives by adjusting the amplitude V_{ac} and phase φ_{ac} of the AC component of arm modulation voltage.

2) 3-Degree-of-Freedom Control

As analyzed in Section IV.B.1), when using the 2 DoF control shown in Fig. 8, the MMC cannot flexibly regulate the DC voltage independently of the AC voltage. Under DC line short-circuit faults, the fault current can surge to extremely high levels within milliseconds, posing a severe threat to system and equipment safety [20][88]. Typically, the fault is isolated by tripping circuit breakers or blocking the converter [89]-[91], as seen in the Zhangbei DC grid project in China.

With the introduction of full-bridge SMs, hybrid MMCs combining full-bridge and half-bridge SMs gain the ability to output negative voltage, enabling active fault current limiting. Leveraging the flexibility of hybrid MMC topology, references [45] and [46] broke through the traditional 2 DoF control by introducing a DC current control, as shown in Fig. 9.

Compared to the 2 DoF control in Fig. 8, the control in Fig. 9 no longer maintains the v_{pj}^{dc} at rated value. Instead, it adds a third modulation signal M_{dc} to adjust v_{pj}^{dc}, which can be termed MMC's 3 DoF control. In this way, the MMC can not only regulate AC voltage amplitude and phase but also directly regulate DC voltage. However, since the NLM still uses V_{CN} as the denominator, the 3 DoF control cannot actively regulate the SM capacitor voltage.

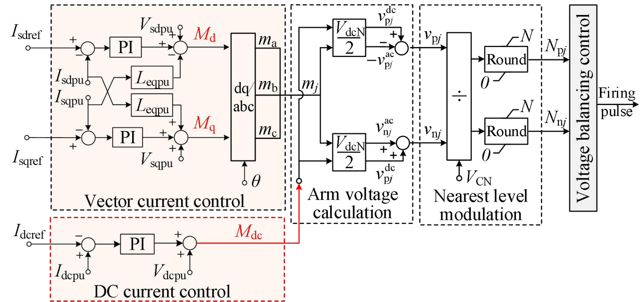

Fig. 9 3-degree-of-freedom-control of MMC.

By directly controlling DC voltage, the MMC can rapidly reduce the DC output voltage during a DC fault, suppressing the DC fault current and enabling fault ride-through without blocking MMC [47]-[49]. References [92] and [93] further designed online entry/exit strategies for MMC, enhancing operational flexibility and reliability [94]. This control architecture has been successfully applied in the Kunliulong DC project in China [95][96].

Additionally, since DC current control can independently regulate DC voltage apart from vector current control, studies [97]-[100] proposed a dual-port voltage control structure based on 3 DoF control, as shown in Fig. 10. This control achieves simultaneous regulation of DC and AC voltages. Although the 2 DoF control architecture in Fig. 8 can also regulate both DC and AC voltages [20], the DC voltage control is coupled with the AC voltage control through the d-axis current control, resulting in slower response times.

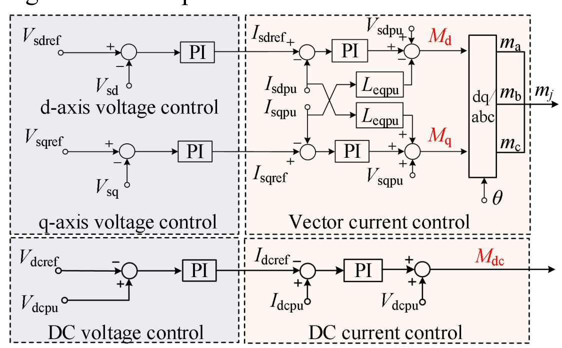

Fig. 10 Dual-port voltage control of MMC.

3) 4-Degree-of-Freedom Control

As analyzed above, in the NLM of 3 DoF control, the rated SM capacitor voltage (V_{CN}) is used as the denominator, which makes it challenging to regulate the SM capacitor voltage. To address this issue, references [59] and [60] propose active energy control to achieve regulation of the SM capacitor voltage. The inner loop control block diagram is shown in Fig. 11. As can be seen, active energy control introduces a capacitor voltage modulation coefficient (M_C) to replace V_{CN} in the 3 DoF control. The M_C is expressed as:

$$M_C = \frac{1}{3}\left(V_{Cavga} + V_{Cavgb} + V_{Cavgc}\right) \qquad (7)$$

where V_{Cavgj} (j = a, b, c) represents the average SM capacitor voltage per phase.

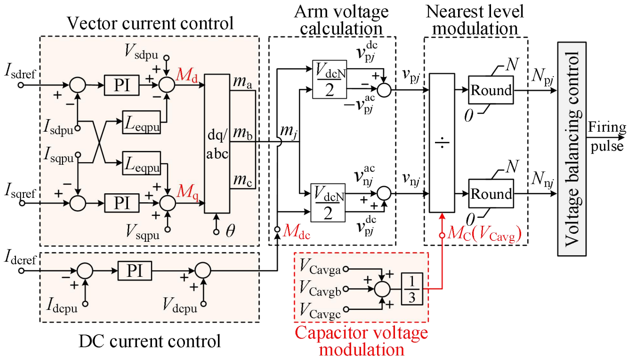

Fig. 11 4-degree-of-freedom control of MMC.

In Fig. 11, the MMC converter includes four modulation coefficients in its control: M_d, M_q, M_{dc}, and M_C. Thus, it can be referred to as the 4 DOF control of MMC. The function of these coefficients can be summarized [60]:

- M_d and M_q are used to regulate the amplitude V_{ac} and phase φ_{ac} of the AC component of arm voltage v_{pj}^{ac} (or v_{nj}^{ac}).
- M_{dc} is responsible for adjusting DC component v_{pj}^{dc} (or v_{nj}^{dc}).
- M_C is to manage SM capacitor voltage V_{Cavgpj} (or V_{Cavgnj}).

Based on the energy regulation capability of the 4 DOF control architecture, an inertia support method utilizing MMC energy has been developed. References [102] and [103] introduced the frequency-energy (*f*-*W*) droop control for MMC to emulate the rotor kinetic energy characteristics of SGs under frequency deviations. Further, references [56] and [57] incorporated short-term frequency regulation control into the *f*-*W* control strategy. However, the duration of energy utilization is very short under major frequency disturbance, leading to a rapid interruption of inertia support, thereby weakening its effectiveness. To address this issue, reference [58] proposed an energy regulation curve based on the rate of change of frequency (RoCoF), which can enhance the inertia support capability of MMC by more than 10%.

V. Analysis of Multi-Degree-of-Freedom Control Framework of HVDC Converters

A. Control Degree of Freedom of HVDC Converters

As analyzed above, continuous advancements in power electronic devices and topologies have significantly enhanced the control flexibility of DC converters. Therefore, this section provides a comprehensive summary of the CDoF in HVDC converters, integrating their topological characteristics and control requirements. A summary of existing multi-degree-of-freedom control strategies for converters is presented in the green-shaded areas of Table I.

The LCC adopts thyristors, which can only be actively turned on but cannot be turned off autonomously. As a result, LCC can only achieve DC voltage regulation by adjusting a single control variable, i.e., the firing angle. Consequently, the control objective of LCC is only to determine the firing angle, which means that the maximum CDoF of LCC is 1.

Compared to LCC, the VSC utilizes fully controllable IGBT devices and PWM technology to generate an AC voltage waveform that matches the AC voltage modulation wave. Thus, the control objective of VSC is to determine AC modulation voltage. Since the AC voltage modulation wave has two variables-amplitude and phase that need to be determined, the maximum CDoF of VSC is 2. Thus, 2 DoF control strategies such as indirect current control, vector current control, and grid-forming control, have already reached the control limits of VSC.

For MMC, each arm is designed with a modular structure and employs NLM techniques. The voltage modulation wave of each arm contains four control variables: AC component (including amplitude and phase), DC component, and SM capacitor voltage. Considering both the upper and lower arms, MMC theoretically has a maximum of 8 CDoF. However, due to the symmetrical modulation approach adopted in current MMC control schemes, the maximum CDoF is limited to 4 in practice. Therefore, the 4 DoF control method illustrated in Fig. 11 represents the control limit of MMC under symmetrical modulation conditions.

B. Control Framework Expansion of MMC

Further considering the asymmetric modulation of MMC, the flexibility of the existing MMC control can be enhanced. From the previous analysis, under symmetric modulation operation, a single arm modulation voltage must be determined, including the amplitude and phase of the AC component, the DC component, and the SM capacitor voltage. In contrast, asymmetric modulation requires determining the voltage modulation waves of both the upper and lower arms separately.

1) AC component modulation: For asymmetric modulation of the AC component, the condition $v_{pj}^{ac} \neq v_{nj}^{ac}$ arises. According to Fig. 7 and (5), MMC's AC-side voltage can be regulated by adjusting either v_{pj}^{ac} and v_{nj}^{ac}, with a control effect equivalent to that of symmetric modulation. However, it will simultaneously introduce a voltage containing both AC and DC components at MMC's DC side. This may result in a significant fundamental frequency AC current flowing between the upper and lower arms, drastically increasing converter valve losses. Additionally, the AC current on the DC side can propagate along the DC transmission line, negatively impacting the stability of other MMCs. Thus, although technically feasible, asymmetric modulation of the AC component is impractical for real-world applications due to its severe impact on system economic efficiency and operational safety. Therefore, this paper does not further explore control structures based on asymmetric AC component modulation.

2) DC component modulation: For asymmetric modulation of the DC component, the condition $v_{pj}^{dc} \neq v_{nj}^{dc}$ arises. According to (5), MMC's DC-side voltage regulation can be achieved by adjusting either v_{pj}^{dc} and v_{nj}^{dc}. Since DC transmission generally operates in a pseudo-bipolar or bipolar mode, asymmetric modulation of the DC component can be used to regulate the positive and negative DC voltages (V_{dcp} and V_{dcn}), enabling independent pole operation under a single-pole fault. However, under this condition, MMC's AC-side voltage will exhibit a DC offset. To mitigate this, the MMC transformer should adopt a high-resistance grounding configuration on the valve side to reduce ground current and minimize operational losses.

In symmetric modulation, the DC component of the arm modulation voltage is controlled by M_{dc}. Therefore, under asymmetric modulation, independent regulation of the DC components of the upper and lower arms requires two separate control variables, M_{dcp} and M_{dcn}. By analogy with the 4 DoF control shown in Fig. 11, the control structure can be extended to the 5 DoF control illustrated in Fig. 12. This expanded control architecture includes five control variables: M_{d}, M_{q}, M_{dcp}, M_{dcn}, and M_{C}.

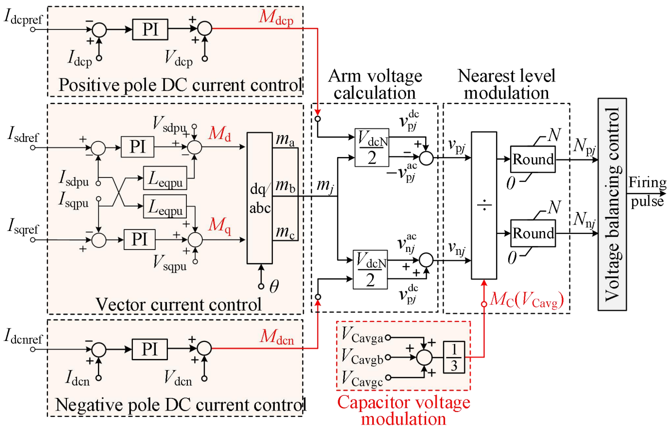

Fig. 12 5-degree-of-freedom control of MMC.

3) Capacitor voltage modulation

For asymmetric modulation of the capacitor voltage, the condition $V_{\mathrm{Cavgp}j} \neq V_{\mathrm{Cavgn}j}$ arises. According to (6), since SMs can be dynamically inserted or bypassed, variations in the SM capacitor voltage do not affect the arm voltage modulation waves. Consequently, it also does not impact MMC's AC and DC voltage. This indicates that asymmetric modulation of the SM capacitor voltage is feasible.

As analyzed above, in a symmetric modulation structure, the SM capacitor voltage in the NLM is determined by M_{C}. Therefore, under asymmetric modulation, to further regulate the SM capacitor voltages of the upper and lower arms, two separate control components, M_{Cp} and M_{Cn}, are required for independent adjustment, respectively:

$$\begin{aligned} M_{\mathrm{Cp}} &= V_{\mathrm{Cavgp}} = \frac{1}{3}\left(V_{\mathrm{Cavgpa}} + V_{\mathrm{Cavgpb}} + V_{\mathrm{Cavgpc}}\right) \\ M_{\mathrm{Cn}} &= V_{\mathrm{Cavgn}} = \frac{1}{3}\left(V_{\mathrm{Cavgna}} + V_{\mathrm{Cavgnb}} + V_{\mathrm{Cavgnc}}\right) \end{aligned} \tag{8}$$

Based on the 5 DOF control shown in Fig. 12, a similar control architecture can be derived to achieve asymmetric modulation of the SM capacitor voltages in the upper and lower arms, as illustrated in Fig. 13. Since this control strategy introduces six independent control variables (M_{d}, M_{q}, M_{dcp}, M_{dcn}, M_{Cp} and M_{Cn}), it is referred to as the 6 DOF control of MMC.

In summary, under asymmetric modulation conditions, the MMC control architecture can be classified as shown in the yellow-highlighted section of TABLE I. From a topological perspective, MMC possesses 8 CDoF. However, asymmetric modulation of the AC voltage would negatively impact the stability of the DC system, making it unsuitable for real-world applications. Therefore, in practical implementations, the maximum achievable control structure for MMC is limited to 6 DOF control.

Regarding the application scenarios of the proposed 6 DoF control strategy, two key advantages can be identified:

Firstly, in MMC-HVDC systems integrating offshore wind farms, when a pole-to-ground DC fault occurs, the proposed 6 DoF control enables the reduction of the faulty pole voltage,

TABLE I
EVOLUTION OF MUTI-DEGREE-OF-FREEDOM CONTROL OF HVDC CONVERTER

<table>
<tr><th>Converter Type</th><th>Converter Topology</th><th colspan="3">Control Requirements</th><th>Control Framework</th><th>Control Variables</th><th>Control Characteristics</th></tr>
<tr><td>Thyristor-Based Converters</td><td>LCC (Centralized)</td><td colspan="3">Requires determination of firing angle (1 CDoF)</td><td>Firing angle control (1 DOF control)</td><td>$\alpha_{\mathrm{r}}/\alpha_{\mathrm{i}}$</td><td>Only control V_{dc}</td></tr>
<tr><td rowspan="7">IGBT-Based Converters</td><td>VSC (Centralized)</td><td colspan="3">Requires determination of AC voltage modulation wave (2 CDoF)</td><td rowspan="2">Indirect current control, Direct current control Grid-forming control (2 DOF control)</td><td rowspan="2">V_{ac}, φ_{ac} (or M_{d}, M_{q})</td><td rowspan="2">Control V_{ac} and φ_{ac}</td></tr>
<tr><td rowspan="6">MMC (Modularized)</td><td rowspan="6">Requires determination of upper and lower arm voltage modulation waves</td><td rowspan="3">Symmetrical modulation, unified upper and lower arms modulation (4 CDoF)</td><td>AC component</td></tr>
<tr><td>DC component</td><td>3 DOF control</td><td>M_{d}, M_{q}, M_{dc}</td><td>Control V_{ac}, φ_{ac}, V_{dc}</td></tr>
<tr><td>Capacitor voltage</td><td>4 DOF control</td><td>M_{d}, M_{q}, M_{dc}, M_{C}</td><td>Control V_{ac}, φ_{ac}, V_{dc}, V_{Cavg}</td></tr>
<tr><td rowspan="3">Asymmetrical modulation, independent upper and lower arm modulation (8 CDoF)</td><td>AC component</td><td></td><td></td><td></td></tr>
<tr><td>DC component</td><td>5 DOF control</td><td>M_{d}, M_{q}, M_{dcp}, M_{dcn}, M_{C}</td><td>Control V_{ac}, φ_{ac}, V_{dcp}, V_{dcn}, V_{Cavg}</td></tr>
<tr><td>Capacitor voltage</td><td>6 DOF control</td><td>M_{d}, M_{q}, M_{dcp}, M_{dcn}, M_{Cp}, M_{Cn}</td><td>Control V_{ac}, φ_{ac}, V_{dcp}, V_{dcn}, V_{Cavgp}, V_{Cavgn}</td></tr>
</table>

allowing the healthy pole to continue transmitting up to 50% of the nominal power. This ensures partial power delivery and avoids complete system shutdown. In contrast, conventional control schemes lacking unipolar operation capability typically lead to full power interruption during such faults.

Secondly, during pole-to-ground faults, the capacitor energy of the faulted arm can be discharged to a lower level than that of the healthy arm. However, conventional symmetric control (e.g., in lower-DoF schemes) limits the energy discharge of the faulted arm to that of the healthy arm, restricting its contribution to fault ride-through. The 6 DoF control relaxes this symmetry constraint and enables asymmetric modulation of arm energy, allowing deeper utilization of the faulted arm's capacitor energy and providing stronger grid support during disturbances.

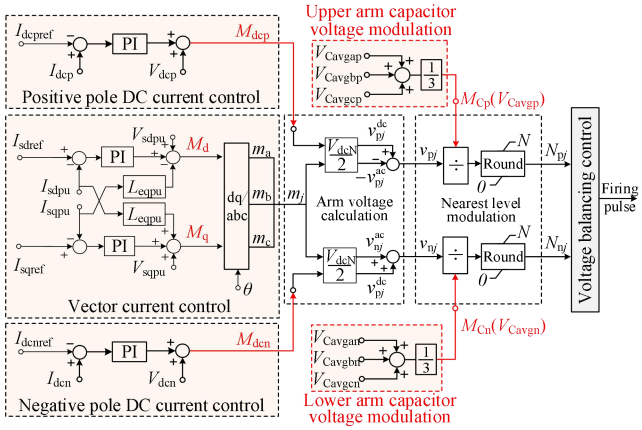

Fig. 13 6-degree-of-freedom control of MMC.

VI. Verification of 6 DoF Control for MMC

Section V provides an outlook on the development of control architectures for MMC. The 6 DoF control of MMC enables separate modulation of DC voltage and SM capacitor voltages. Therefore, to verify the control capability of 6 DoF control, a two-terminal half-bridge MMC-HVDC system, as shown in Fig. 14, was built in the PSCAD/EMTDC. In this system, MMC1 operates as a constant power station, while MMC2 functions as a constant DC voltage station. The system simulation parameters are provided in Table II.

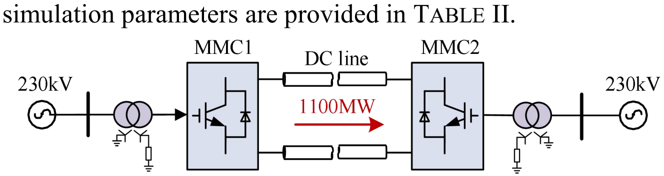

Fig. 14 Two-terminal MMC-HVDC system.

Both MMC1 and MMC2 adopt the 6 DoF control shown in Fig. 13. The outer-loop control structures for MMC1 and MMC2 are illustrated in Fig. 15 (a) and (b), respectively. In particular, MMC1 not only employs constant power control but also incorporates capacitor energy control for the upper and lower arms, allowing independent regulation of the SM capacitor voltages in the upper and lower arms. Meanwhile, MMC2 is designed with independent DC voltage control for the positive and negative poles, enabling separate regulation of the positive and negative-pole DC voltages. The detailed design of the controllers can be found in [59], which discusses capacitor energy and DC voltage control under symmetric modulation. Hence, it will not be elaborated further in this paper.

Table II
System Parameters of MMC-HVDC

Parameters		MMC1	MMC2
Rated capacity/MVA		1100	1100
DC voltage/kV		±400	±400
Number of SMs per arm		400	400
SM capacitance/μF		9000	9000
Arm reactance/mH		133	133
Transformer	Voltage ratio	230/416.41	230/416.41
	Leakage reactance /%	17	14
DC line	Length/km	108	
	Capacitance/μF	19.53	

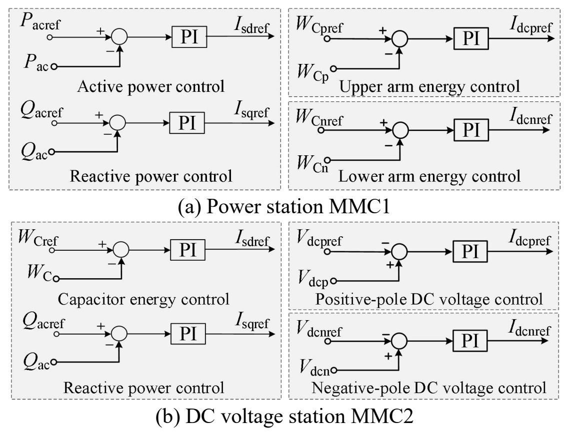

Fig. 15 6-degree-of-freedom control for MMC-HVDC system.

A. Performance of Asymmetric DC Voltage Control

To verify the independent pole control capability of the 6 DoF control, the control reference of the constant DC voltage station MMC2 was adjusted at t=2.0s and t=2.4s. The positive-pole DC voltage was increased from the rated value of 400 kV to 460 kV and decreased to 340 kV, respectively. Meanwhile, the negative-pole DC voltage was maintained constant. The results are shown in Fig. 16.

Fig. 16 (a) presents the waveforms of the positive and negative DC link voltages. It can be observed that the positive DC voltage changes according to the predefined regulation, while the negative DC voltage remains stable at its rated value of -400 kV. This confirms that under 6 DoF control, the MMC can achieve asymmetric control of the positive and negative DC voltages.

Fig. 16 (b) and (c) show the AC voltage waveforms on the transformer grid side and valve side of MMC2, respectively. It can be seen that during asymmetric DC voltage operation, there is a DC offset in the valve-side AC voltage (V_c). However, due to the isolation effect of the transformer, the grid-side AC voltage does not exhibit a DC offset, ensuring the stable operation of the system.

Fig. 16 (d) displays the capacitor voltage waveforms of the MMC upper and lower arm SMs. During asymmetric DC voltage operation, the SM capacitor voltages remain unaffected. Fig. 16 (e) presents the waveforms of the positive and negative-pole DC currents of the MMC. Since the system transmission power remains unchanged, the DC current varies accordingly with changes in the positive-pole DC voltage, and the variations in the positive and negative-pole DC currents are identical.

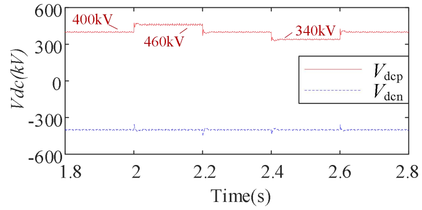

(a) Positive and negative-pole DC voltage

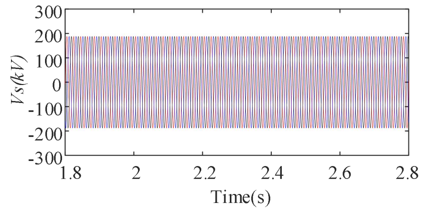

(b) AC voltage at grid side of the transformer

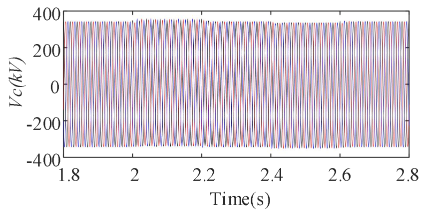

(c) AC voltage at valve side of the transformer

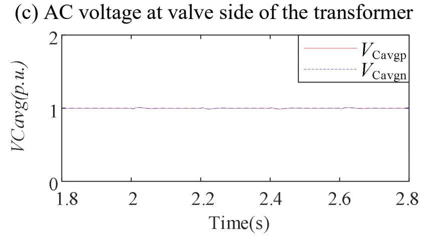

(d) SM capacitor voltage

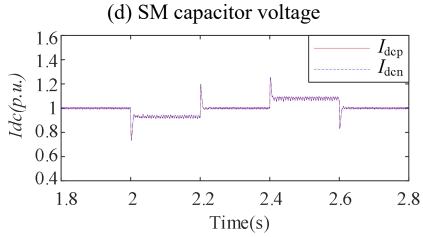

(e) Positive and negative-pole DC current

Fig. 16 Results of asymmetric DC voltage control.

B. *Performance of Asymmetric SM Capacitor Voltage Control*

To further verify the capability of the 6 DoF control in the asymmetric operation of SM capacitor voltages, the energy control reference of MMC1 was adjusted at *t*=3.0s and *t*=3.4s. Decrease the upper arm capacitor energy from the rated value of 0.5p.u. to 0.4p.u. and then increase to 0.6p.u., respectively. Meanwhile, the lower arm capacitor energy remained unchanged. The simulation results are shown in Fig. 17.

Fig. 17 (a) and (b) present the upper and lower arm capacitor energy and SM capacitor voltage of MMC1. The results show that MMC1 accurately regulates the upper arm capacitor energy to the predefined values while maintaining the lower arm capacitor energy and SM capacitor voltage at the rated value. This confirms that under 6 DoF control, MMC1 can achieve asymmetric control of the upper and lower arm SM capacitor voltages.

Fig. 17 (c) and (d) illustrate the AC voltage at the grid side and valve side of the MMC1 transformer. It can be observed that during the energy regulation process, neither the grid-side nor the valve-side AC voltage exhibits a DC offset, ensuring stable system operation. Fig. 17 (e) shows the positive and negative-pole DC voltages. The results indicate that the DC voltage experiences only transient fluctuations at the moment of energy variation and then quickly stabilizes at the rated value. This confirms that the asymmetric adjustment of capacitor voltage (energy) does not affect the AC and DC side voltages.

Fig. 17 (f) presents the positive and negative-pole DC current of MMC1. It can be seen that significant fluctuations occur in the DC currents to facilitate the asymmetric adjustment of upper and lower arm capacitor voltages, and the variation trends of the positive and negative DC currents are different. Fig. 17 (g) displays MMC1's AC and DC power. The AC power P_{ac} remains steady at the rated value of 1.0 p.u., while during the decrease (or increase) of MMC1's energy, the DC power P_{dc} decreases (or increases) accordingly. During this period, the power imbalance between P_{ac} and P_{dc} is entirely from the upper arm capacitor energy of MMC1.

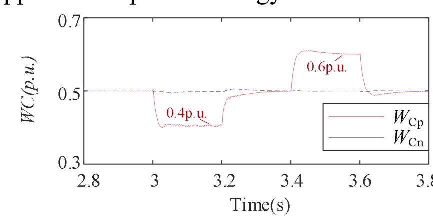

(a) Upper and lower arm capacitor energy

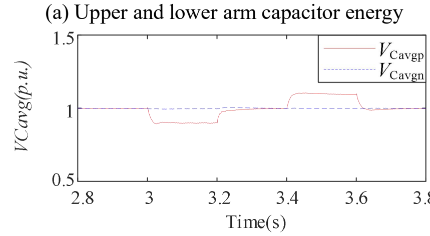

(b) SM capacitor voltage

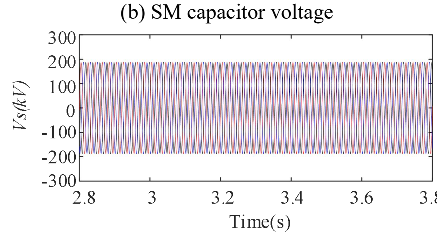

(c) AC voltage at grid side of the transformer

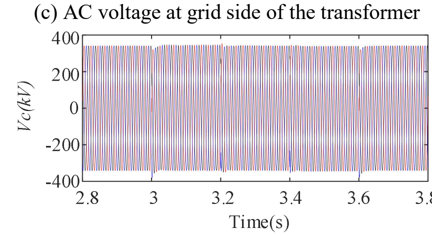

(d) AC voltage at valve side of the transformer

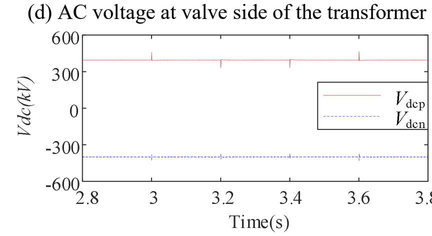

(e) Positive and negative-pole DC voltage

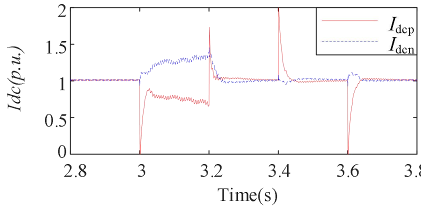

(f) Positive and negative-pole DC current

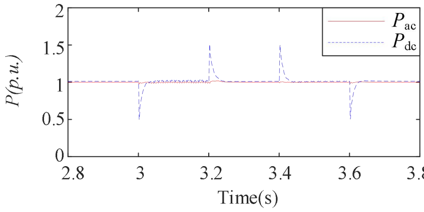

(g) AC and DC power

Fig. 17 Results of asymmetric SM capacitor voltage control.

VII. Control Degree of Freedom Requirements for Grid-Forming MMC-HVDC

As the penetration of renewable energy continues to rise, the grid-forming control of MMC will become a key factor in ensuring stable operation when integrating weak AC power grids. The essence of grid-forming control lies in the converter's ability to autonomously establish AC voltage, and maintain its amplitude and frequency to support the power grid.

Grid-forming control primarily mimics the operating characteristics of SGs. Fig. 18 (a) shows the principle of grid support from an SG under grid disturbances. During voltage disturbances, the SG regulates the rotor flux linkage ψ via the excitation system to stabilize the stator-induced EMF (E_q), thereby automatically generating reactive power Q_{ac} to support the stability of terminal voltage V_{ac}. Simultaneously, the generator relies on the release of kinetic energy W_K from the rotor to provide active power P_{ac} support in the short term, ensuring the stability of terminal frequency ω_{ac}.

According to the above analysis, to achieve the gird forming capability, the devices must have an energy reserve to provide support power for the grid to maintain stable AC voltage and frequency.

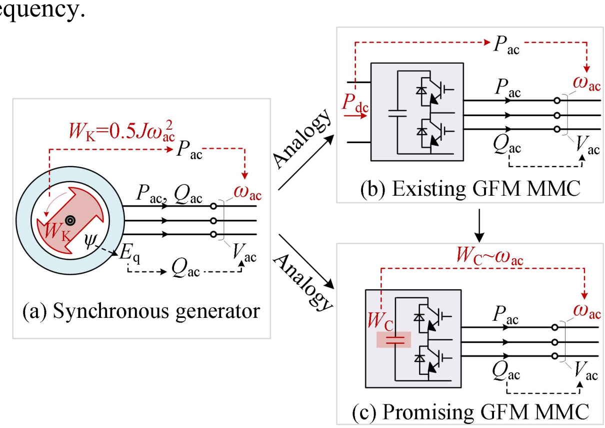

Fig. 18 Energy sources for grid support in grid-forming devices.

By analogy with SGs, the existing grid-forming control for MMC-HVDC is primarily based on 2 DoF control, which autonomously establishes AC voltage. It provides frequency and voltage support through power synchronization control (P_{ac}~ω_{ac}) and reactive power-voltage control (Q_{ac}~V_{ac}). This principle is illustrated in Fig. 18 (b). When the converter's output voltage V_{ac} experiences disturbances, the MMC adjusts its reactive power Q_{ac} to provide voltage support, as indicated by the black dashed line in Fig. 18 (b). Similarly, when the frequency ω_{ac} fluctuates, the MMC adjusts its active power P_{ac} to provide frequency support, as shown by the red dashed line.

Although 2 DoF grid-forming control has been widely applied, its limitations are becoming increasingly apparent. First, it underutilizes control flexibility since it does not leverage the energy stored in MMC capacitors. Instead, all the energy required for grid-forming depends on the DC side or the sending-end power source, as illustrated by P_{dc} in Fig. 18 (b). This means that if the DC side or sending-end power source is unstable, the grid-forming capability of the HVDC system will be constrained. Additionally, in power systems with a high penetration of renewable energy, both the sending and receiving ends of an HVDC system may be weak grids, requiring simultaneous support at both ends. However, traditional 2 DoF control relies on external power sources, meaning that if the HVDC system lacks an external power supply, it will struggle to effectively provide grid support. Thus, future power systems will need to rely on the intrinsic grid-forming capability of the HVDC itself rather than external power sources.

MMC multi-DoF control enables regulation of internal capacitor energy, allowing MMC capacitor energy to provide short-term support power for grid-forming. By drawing an analogy with SGs, the relationship between kinetic energy W_K and frequency ω_{ac} (rotor speed) is established:

$$W_K = 0.5J\omega_{ac}^2 \tag{9}$$

where J represents the rotor inertia of the generator rotor. To utilize internal energy for frequency stability like SGs, the MMC capacitor energy W_C can be coupled with AC grid frequency ω_{ac}, as shown in Fig. 18 (c).

Considering that 4 DoF control allows for energy regulation, studies [99] and [59] have proposed two different energy synchronization control methods (W_C~ω_{ac}) based on 4 DoF control, as illustrated in Fig. 19 (a) and (b). Both methods introduce an additional energy control loop, enabling MMC to fully utilize capacitor energy for short-term power support, thereby enhancing grid-forming capability and reducing reliance on external energy sources. The comparisons between these two energy synchronization control schemes can be summarized in Table III according to reference [59].

Table III
Comparisons Between Two Energy Synchronization Control

Category	Type I	Type II
Principle	Based on rotor–capacitor energy analogy	Based on energy–power dynamics
Frequency Dependence	Dependent on grid frequency	Independent of grid frequency
Flexibility	Limited under large frequency changes	High; allows optimized energy use
Complexity	Simple to implement	Requires more complex parameter tuning
Limitation	Risk of energy exceeding limits during frequency drift	Higher tuning burden

In summary, traditional 2 DoF grid-forming control is constrained by its limited control flexibility, which can solely achieve power-based grid-forming. This control has inherent limitations in terms of independent grid-forming capability, making it insufficient to meet the operational demands of weak grids. To address this issue, the MMC control architecture must adopt an energy-based grid-forming method, which requires the use of at least 4 CDoF to effectively utilize SM capacitor energy.

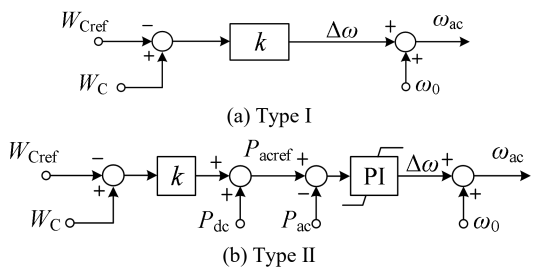

Fig. 19 Energy synchronization control of MMC.

VIII. Conclusion

By analyzing the topological characteristics and control requirements of different converters, this paper summarizes the control architecture of existing HVDC converters as follows:

1) LCC converters use thyristor-based semi-controlled devices, which can only be turned on but not actively turned off. As a result, LCCs have only 1 CDoF, the firing angle (α). All control strategies for LCCs are designed around this single control variable, allowing only DC voltage regulation.
2) VSC converters use fully controllable IGBT devices and PWM technology. During normal operation, the control system generates an AC modulation wave (m_j) to create the corresponding voltage wave at the AC side. Therefore, VSC control strategies are all designed based on 2 CDoF (i.e., the amplitude V_{ac} and phase φ_{ac}).
3) MMC converters adopt a modular topology and NLM technology. During operation, the control system must determine modulation voltages of the upper and lower arms, which consists of eight control variables: the amplitude (V_{acp} and V_{acn}) and phase (φ_{acp} and φ_{acn}) of the AC components, the DC components (v_{pj}^{dc} and v_{nj}^{dc}), and the average capacitor voltages of the SMs ($V_{\mathrm{Cavgp}j}$ and $V_{\mathrm{Cavgn}j}$). As a result, all MMC control strategies must be designed around these 8 CDoF.

However, current MMC control adopt symmetrical modulation of the upper and lower arms, restricting MMC control to only 4 CDoF. To overcome this limitation while ensuring operational feasibility, this paper proposes a 6 DoF control framework. Simulation results demonstrate that, compared to the conventional 4 DoF control, the proposed 6 DoF control enables asymmetric regulation of DC voltage and SM capacitor voltage, improving control flexibility.

Finally, this paper discusses the CDoF requirements for grid-forming MMC. The analysis reveals that existing grid-forming control strategies rely on 2 DoF control, which only supports power-based grid-forming and lacks independent grid-forming capability. To address this, at least 4 CDoF are required to achieve an energy-based grid-forming capability of MMC to fully utilize the internal energy for enhancing grid support performance.

References

[1] L. Liu, D. Ke, N. Zeng, et al., “The study of fuzzy controller in MTDC system,” *Power Syst. Technol.*, vol. 22, no. 9, pp. 22–26, 1998.

[2] T. Machida, Y. Yoshida, “A method to detect the deionization margin angle and to prevent the commutation failure of an inverter for dc transmission,” *IEEE Trans. Power App. Syst.*, no. 3, pp. 259–262, 1967.

[3] V. K. Sood, HVDC and FACTS Controllers: Applications of Static Converters in Power Systems. Springer Science & Business Media, 2006.

[4] S. Tamai, H. Naitoh, F. Ishiguro, et al., “Fast and predictive HVDC extinction angle control,” *IEEE Trans. Power Syst.*, vol. 12, no. 3, pp. 1268–1275, 1997.

[5] J. V. Wijayakulasooriya, G. A. Putrus, C. H. Ng, “Fast non-recursive extraction of individual harmonics using artificial neural networks,” *IEE Proc.-Gener. Transm. Distrib.*, vol. 152, no. 4, pp. 539–543, 2005.

[6] A. Hansen, H. Havemann, “Decreasing the commutation failure frequency in HVDC transmission systems,” *IEEE Trans. Power Del.*, vol. 15, no. 3, pp. 1022–1026, 2000.

[7] L. Zhang, L. Dofnas, “A novel method to mitigate commutation failures in HVDC systems,” *in Proc. Int. Conf. Power Syst. Technol.*, vol. 1, pp. 51–56, 2002.

[8] Z. Wei, Y. Yuan, X. Lei, et al., “Direct-current predictive control strategy for inhibiting commutation failure in HVDC converter,” *IEEE Trans. Power Syst.*, vol. 29, no. 5, pp. 2409–2417, 2014.

[9] S. Mirsaeidi, D. Tzelepis, J. He, et al., “A controllable thyristor-based commutation failure inhibitor for LCC-HVDC transmission systems,” *IEEE Trans. Power Electron.*, vol. 36, no. 4, pp. 3781–3792, 2020.

[10] R. Li, S. Bozhko and G. Asher, “Frequency Control Design for Offshore Wind Farm Grid With LCC-HVDC Link Connection,” *IEEE Trans. Power Electron.*, vol. 23, no. 3, pp. 1085-1092, May 2008.

[11] G.-S. Lee, D.-H. Kwon, S.-I. Moon, et al., “A coordinated control strategy for LCC HVDC systems for frequency support with suppression of AC voltage fluctuations,” *IEEE Trans. Power Syst.*, vol. 35, no. 4, pp. 2804–2815, July 2020.

[12] Y. Xue, Y. Chen, W. Zheng, et al., “Sharing of Primary Frequency Response Using LCC-HVDC,” *IEEE Trans. Power Del.*, vol. 39, no. 4, pp. 2457-2469, Aug. 2024.

[13] D. -H. Kwon, Y. -J. Kim and O. Gomis-Bellmunt, “Optimal DC Voltage and Current Control of an LCC HVDC System to Improve Real-Time Frequency Regulation in Rectifier- and Inverter-Side Grids,” *IEEE Trans. Power Syst.*, vol. 35, no. 6, pp. 4539-4553, Nov. 2020.

[14] L. Wang and M. S. -N. Thi, “Comparisons of Damping Controllers for Stability Enhancement of an Offshore Wind Farm Fed to an OMIB System Through an LCC-HVDC Link,” *IEEE Trans. Power Syst.*, vol. 28, no. 2, pp. 1870-1878, May 2013.

[15] L. Peng, Y. Xu, A. H. Abolmasoumi, et al., “AC/DC Hybrid Power System Damping Control Based on Estimated Model Predictive Control Considering the Real-Time LCC-HVDC Stability,” *IEEE Trans. Power Syst.*, vol. 39, no. 1, pp. 506-516, Jan. 2024.

[16] R. Eriksson, “On the centralized nonlinear control of HVDC systems using Lyapunov theory,” *IEEE Trans. Power Del.*, vol. 28, no. 2, pp. 1156–1163, April 2013.

[17] B. T. Ooi, X. Wang, “Boost-type PWM HVDC transmission system,” *IEEE Trans. Power Del.*, vol. 6, no. 4, pp. 1557–1563, 1991.

[18] B. T. Ooi, X. Wang, “Voltage angle lock loop control of the boost type PWM converter for HVDC application,” *IEEE Trans. Power Electron.*, vol. 5, no. 2, pp. 229–235, 1990.

[19] W. Lu, B. T. Ooi, “Multi-terminal LVDC system for optimal acquisition of power in wind-farm using induction generators,” in *Proc. IEEE 32nd Annu. Power Electron. Spec. Conf.*, vol. 1, pp. 210–215, 2001.

[20] Z. Xu, Flexible HVDC Transmission Systems. Beijing: Mechanical Industry Press, 2016.

[21] W. Du, Z. Chen, K. P. Schneider, et al., “A comparative study of two widely used grid-forming droop controls on microgrid small-signal stability,” *IEEE J. Emerg. Sel. Topics Power Electron.*, vol. 8, no. 2, pp. 963–975, 2019.

[22] Y. Wang, W. Xiang, H. Zhang, et al., “Optimal Allocation of Grid-forming and Grid-following WTGs for Stable Weak Grid Integration,” *CSEE J. Power & Energy*, early access, to be published.

[23] L. Zhang, L. Harnefors, H.-P. Nee, "Power-synchronization control of grid-connected voltage-source converters," *IEEE Trans. Power Syst.*, vol. 25, no. 2, pp. 809–820, 2010.

[24] S. D'Arco, J. A. Suul, "Virtual synchronous machines—Classification of implementations and analysis of equivalence to droop controllers for microgrids," *in Proc. IEEE Grenoble Conf.*, pp. 1–7, 2013.

[25] N. Pogaku, M. Prodanovic, T. C. Green, "Modeling, analysis and testing of autonomous operation of an inverter-based microgrid," *IEEE Trans. Power Electron.*, vol. 22, no. 2, pp. 613–625, 2007.

[26] P. Hart, B. Lesieutre, "Energy function for a grid-tied, droop-controlled inverter," *in Proc. North Amer. Power Symp*., pp. 1–6, 2014.

[27] Q.-C. Zhong, "Virtual synchronous machines: A unified interface for grid integration," *IEEE Power Electron. Mag*., vol. 3, no. 4, pp. 18–27, 2016.

[28] Q.-C. Zhong, P.-L. Nguyen, Z. Ma, et al., "Self-synchronized synchronverters: Inverters without a dedicated synchronization unit," *IEEE Trans. Power Electron.*, vol. 29, no. 2, pp. 617–630, 2013.

[29] W. Zhang, A. M. Cantarellas, J. Rocabert, et al., "Synchronous power controller with flexible droop characteristics for renewable power generation systems," *IEEE Trans. Sustain. Energy*, vol. 7, no. 4, pp. 1572–1582, 2016.

[30] P. Rodriguez, I. Candela, A. Luna, "Control of PV generation systems using the synchronous power controller," *in Proc. IEEE Energy Convers. Congr. Expo.*, pp. 993–998, 2013.

[31] W. Zhang, D. Remon, P. Rodriguez, "Frequency support characteristics of grid-interactive power converters based on the synchronous power controller," *IET Renew. Power Gener.*, vol. 11, no. 4, pp. 470–479, 2016.

[32] L. Huang, H. Xin, Z. Wang, et al., "A virtual synchronous control for voltage-source converters utilizing dynamics of DC-link capacitor to realize self-synchronization," *IEEE J. Emerg. Sel. Topics Power Electron.*, vol. 5, no. 4, pp. 1565–1577, 2017.

[33] O. D. Adeuyi, M. Cheah-Mane, J. Liang, et al., "Fast frequency response from offshore multiterminal VSC–HVDC schemes," *IEEE Trans. Power Del.*, vol. 32, no. 6, pp. 2442–2452, 2016.

[34] I. Cvetkovic, D. Boroyevich, R. Burgos, et al., "Modeling and control of grid-connected voltage-source converters emulating isotropic and anisotropic synchronous machines," *in Proc. IEEE Workshop Control Model. Power Electron*., pp. 1–5, 2015.

[35] F. Milano, F. Dörfler, G. Hug, et al., "Foundations and challenges of low-inertia systems," *in Proc. Power Syst. Comput. Conf.*, pp. 1–25, 2018.

[36] B. B. Johnson, S. V. Dhople, A. O. Hamadeh, et al., "Synchronization of parallel single-phase inverters with virtual oscillator control," *IEEE Trans. Power Electron.*, vol. 29, no. 11, pp. 6124–6138, 2013.

[37] B. B. Johnson, M. Sinha, N. G. Ainsworth, et al., "Synthesizing virtual oscillators to control islanded inverters," *IEEE Trans. Power Electron*., vol. 31, no. 8, pp. 6002–6015, 2015.

[38] M. Sinha, F. Dörfler, B. B. Johnson, et al., "Uncovering droop control laws embedded within the nonlinear dynamics of van der pol oscillators," *IEEE Trans. Control Netw. Syst.*, vol. 4, no. 2, pp. 347–358, 2015.

[39] B. Johnson, M. Rodriguez, M. Sinha, et al., "Comparison of virtual oscillator and droop control," *in Proc. IEEE Workshop Control Model. Power Electron*., pp. 1–6, 2017.

[40] Z. Shi, H. I. Nurdin, J. E. Fletcher, et al., "Similarities between virtual oscillator controlled and droop controlled three-phase inverters," *in Proc. IEEE Int. Power Electron. Motion Control Conf.*, pp. 434–439, 2018.

[41] Z. Shi, J. Li, H. I. Nurdin, et al., "Comparison of virtual oscillator and droop controlled islanded three-phase microgrids," *IEEE Trans. Energy Convers.*, vol. 34, no. 4, pp. 1769–1780, 2019.

[42] P. Hazra, R. Hadidi, E. Makram, "Dynamic study of virtual oscillator controlled inverter based distributed energy source," *in Proc. North Amer. Power Symp*., pp. 1–6, 2015.

[43] D. Raisz, T. T. Thai, A. Monti, "Power control of virtual oscillator controlled inverters in grid-connected mode," *IEEE Trans. Power Electron.*, vol. 34, no. 6, pp. 5916–5926, 2018.

[44] M. A. Awal, H. Yu, H. Tu, et al., "Hierarchical control for virtual oscillator based grid-connected and islanded microgrids," *IEEE Trans. Power Electron.*, vol. 35, no. 1, pp. 988–1001, 2019.

[45] W. Lin, X. Xiang, J. Wen, "A decoupling control method and its application in flexible HVDC transmission systems," Chinese Patent CN106505642A, Mar. 15, 2017.

[46] W. Xiang, W. Lin, L. Xu, et al., "Enhanced independent pole control of hybrid MMC-HVDC system," *IEEE Trans. Power Del.*, vol. 33, no. 2, pp. 861–872, 2018.

[47] M. Zhou, X. Xiang, W. Zuo, et al., "Research on DC fault isolation of MMC based DC Grid using the active current-limiting approach," *Proc. CSEE*, vol. 39, no. 23, pp. 6852–6866, 2019.

[48] G. Li, X. Wang, S. Jiang, et al., "Coordinated Control Strategy of Fault Ride-through for DC Grid Based on Hybrid MMC," *Power Syst. Technol.*, vol. 48, no. 12, pp. 4817–4825, 2024.

[49] W. Han, R. Yang, C. Liu, et al., "DC Fault characteristics and fault current suppression strategy of three-terminal hybrid HVDC system based on LCC and hybrid MMC," *High Volt. Appar.*, vol. 57, no. 6, pp. 179–188, 2021.

[50] A. Antonios, L. Lennart, N. Hans-Peter, "On dynamics and voltage control of the modular multilevel converter," *in Proc. Eur. Conf. Power Electron. Appl.*, pp. 1–10, 2009.

[51] S. Fan, K. Zhang, J. Xiong, et al., "An improved control system for modular multilevel converters with new modulation strategy and voltage balancing control," *IEEE Trans. Power Electron.*, vol. 30, no. 1, pp. 358–371, 2015.

[52] H. Saad, X. Guillaud, J. Mahseredjian, et al., "MMC capacitor voltage decoupling and balancing controls," *IEEE Trans. Power Del*., vol. 30, no. 2, pp. 704–712, 2014.

[53] W. Xiang, J. Wen, H. Zhang, et al., "Three-degree control of MMC based high voltage direct current transmission system," *Power Syst. Technol*., vol. 47, no. 8, pp. 3385–3395, 2023.

[54] H. Zhang, W. Xiang, J. Wen, et al., "Active energy control of offshore wind power MMC-HVDC system to handle AC faults of receiving-end power grid," *Proc. CSEE*, vol. 43, no. 12, pp. 4600–4613, 2023.

[55] H. Zhang, W. Xiang, M. Zhou, et al., "Cooperative strategy of active energy control and AC energy dissipation device in offshore wind power MMC-HVDC system," *Proc. CSEE*, vol. 42, no. 12, pp. 4319–4329, 2022.

[56] A. E. Leon, "Short-term frequency regulation and inertia emulation using an MMC-based MTDC system," *IEEE Trans. Power Syst.*, vol. 33, no. 3, pp. 2854–2863, 2017.

[57] A. E. Leon and J. Freytes, "Dual control structure of modular multilevel converters for power system support," *IEEE Syst. J.*, vol. 16, no. 1, pp. 1602–1605, 2021.

[58] H. Zhang, W. Xiang, Y. He, et al., "Optimal energy utilization of MMC-HVDC system integrating offshore wind farms for onshore weak grid inertia support," *IEEE Trans. Power Syst.*, vol. 39, no. 1, pp. 1304–1318, 2024.

[59] H. Zhang, W. Xiang, J. Wen, "Dual grid-forming control with energy regulation capability of MMC-HVDC system integrating offshore wind farms and weak grids," *IEEE Trans. Power Syst.*, vol. 39, no. 1, pp. 261–272, 2024.

[60] J. Wen, H. Zhang, W. Xiang, et al., "Unified control architecture of flexible DC converters for new-type power systems," *Proc. CSEE*, vol. 44, no. 18, pp. 7068–7084, 2024.

[61] R. Yang, G. Shi, C. Zhang, et al., "Internal energy based grid-forming control for MMC-HVDC systems with wind farm integration," *IEEE Trans. Ind. Appl.*, vol. 59, no. 1, pp. 503–512, 2022.

[62] Z. Yang, M. Li, X. Lu, et al. "Interconnection of VSC-HVDC and LCC-HVDC using DC-DC autotransformer". *The Journal of Engineering*, vol. 2019, no.18, pp: 5033-5037, June 2019.

[63] L. Wang, K. H. Wang, "Dynamic stability analysis of a DFIG-based offshore wind farm connected to a power grid through an HVDC link," *IEEE Trans. Power Syst.*, vol. 26, no. 3, pp. 1501–1510, 2010.

[64] H. Yin, L. Fan, Z. Miao, "Coordination between DFIG-based wind farm and LCC-HVDC transmission considering limiting factors," in Proc. *IEEE EnergyTech*, pp. 1–6, 2011.

[65] C. V. Thio, J. B. Davies, K. L. Kent, "Commutation failures in HVDC transmission systems," *IEEE Trans. Power Del.*, vol. 11, no. 2, pp. 946–957, 1996.

[66] J. Zhu, Y. Li, X. Duan, "Application of SFCLs to inhibit commutation failure in HVDC systems: Position comparison and resistance recommendation," *Can. J. Elect. Comput. Eng.*, vol. 40, no. 1, pp. 31–40, 2017.

[67] S. Mirsaeidi, D. Tzelepis, J. He, et al., "A controllable thyristor-based commutation failure inhibitor for LCC-HVDC transmission systems," *IEEE Trans. Power Electron.*, vol. 36, no. 4, pp. 3781–3792, 2020.

[68] C. Zhang, X. Zhang, PWM Rectifiers and Their Control. Beijing: Mechanical Industry Press, 2003.

[69] H. Zhang, W. Xiang, W. Lin and J. Wen, “Grid Forming Converters in Renewable Energy Sources Dominated Power Grid: Control Strategy, Stability, Application, and Challenges,” *J. Mod. Power Syst. Clean Energy*, vol. 9, no. 6, pp. 1239-1256, Nov. 2021
[70] Q. Wang, J. Ding, H. Liu, et al., “Feasibility of third harmonic injection modulation strategy for MMC-HVDC transmission system,” *Autom. Electr. Power Syst.*, vol. 42, no. 17, pp. 104–110, 2018.
[71] H. Sun, J. Huang, L. Ma, “Analysis and optimization on third harmonic injection strategy for steady-state operation of modular multilevel converter,” *J. North China Electr. Power Univ.*, vol. 47, no. 6, pp. 32–41, 2020.
[72] B. Yuan, N. Mei, D. Chen, et al., “Influences of third harmonic injection on the operation characteristics of MMC system,” *High Volt. Eng.*, vol. 46, no. 3, pp. 1060–1068, 2020.
[73] Y. Xiong, “Active frequency support control of voltage source converter-based multi-terminal direct current system integrated offshore wind farms,” Ph.D. dissertation, Huazhong Univ. Sci. Technol., Wuhan, China, 2022.
[74] W. Yao, Y. Xiong, Y. Han, et al., “Review of voltage source converter-based high voltage direct current integrated offshore wind farm on providing frequency support control,” *High Volt. Eng.*, vol. 47, no. 10, pp. 3397–3413, 2021.
[75] J. Yan, T. Bi, Y. Xu, et al., “An improved frequency control strategy for offshore wind farm connected by VSC-HVDC,” *J. North China Electr. Power Univ.*, vol. 48, no. 2, pp. 11–19, 2021.
[76] Y. Yao, W. Yao, Y. Xiong, et al., “Coordinated frequency support and wind turbine preset restoration scheme of VSC-MTDC integrated offshore wind farms,” *High Volt. Eng.*, vol. 47, no. 10, pp. 3537–3548, 2021.
[77] Y. Lin, Y. Tang, J. Ou, et al., “Quantitative analysis on voltage support strength of offshore wind power grid-connected system via VSC-HVDC considering the influence of sending-side grid,” *Power Syst. Technol.*, vol. 48, no. 11, pp. 4524–4533, 2024.
[78] F. Ma, H. Xin, C. Liu, et al., “Small-disturbance system voltage support strength assessment method for renewables VSC-HVDC delivery system,” *Trans. China Electrotech. Soc.*, vol. 38, no. 21, pp. 5758–5770, 2023.
[79] L. Zhu, Z. Yuan, C. Sheng, et al., “Principle and method of improving short circuit ratio of LCC-HVDC through VSC-HVDC,” *Southern Power Syst. Technol.*, vol. 11, no. 11, pp. 13–19, 2017.
[80] X. Zhai, Z. Guo, J. Wu, “Research on vulnerability of AC converter bus based on short-circuit ratio in VSC-HVDC,” *Electr. Appl.*, vol. 34, no. 14, pp. 121–125, 2015.
[81] R. Eriksson, “On the centralized nonlinear control of HVDC systems using Lyapunov theory,” *IEEE Trans. Power Del.*, vol. 28, no. 2, pp. 1156–1163, 2013.
[82] J. C. Gonzalez-Torres, G. Damm, V. Costan, et al., “A novel distributed supplementary control of multi-terminal VSC-HVDC grids for rotor angle stability enhancement of AC/DC systems,” *IEEE Trans. Power Syst.*, vol. 36, no. 1, pp. 623–634, 2020.
[83] R. Eriksson, “Coordinated control of multiterminal DC grid power injections for improved rotor-angle stability based on Lyapunov theory,” *IEEE Trans. Power Del*., vol. 29, no. 4, pp. 1789–1797, 2013.
[84] J. Renedo, L. Garcıa, L. Rouco, “Active power control strategies for transient stability enhancement of AC/DC grids with VSC-HVDC multi-terminal systems,” *IEEE Trans. Power Syst*., vol. 31, no. 6, pp. 4595–4604, 2016.
[85] G. Tang, Z. Xu, H. Dong, et al., “Sliding mode robust control based active-power modulation of multi-terminal HVDC transmissions,” *IEEE Trans. Power Syst*., vol. 31, no. 2, pp. 1614–1623, 2015.
[86] A. Fuchs, M. Imhof, T. Demiray, et al., “Stabilization of large power systems using VSC–HVDC and model predictive control,” *IEEE Trans. Power Del.*, vol. 29, no. 1, pp. 480–488, 2013.
[87] I. M. Sanz, B. Chaudhuri, G. Strbac, “Coordinated corrective control for transient stability enhancement in future Great Britain transmission system,” *in Proc. Power Syst. Comput. Conf.*, pp. 1–7, 2016.
[88] W. Xiang, W. Lin, J. Wen, et al., “A new topology of sub-modules with dc fault current blocking capability and a new type of hybrid MMC converter,” *Proc. CSEE*, vol. 34, no. 29, pp. 5171–5179, 2014.
[89] J. Wu, L. Yao, Z. Wang, et al., “The study of mmc topologies and their DC Fault current blocking capacities in DC Grid,” *Proc. CSEE*, vol. 35, no. 11, pp. 2681–2694, 2015.
[90] B. Li, J. He, Y. Li, et al., “DC fault protection strategy for the flexible multi-terminal DC system,” *Proc. CSEE*, vol. 36, no. 17, pp. 4627–4637, 2016.
[91] D. Jovcic, G. Tang, H. Pang, “Adopting circuit breakers for high-voltage DC networks: Appropriating the vast advantages of DC transmission grids,” *IEEE Power Energy Mag.*, vol. 17, no. 3, pp. 82–93, 2019.
[92] J. Lu, Y. Dong, Q. Zhang, et al., “Valve group online entry strategy for VSC-UHVDC system based on DC modulation degree,” *Electr. Power Eng. Technol.*, vol. 40, no. 2, pp. 154–161, 2021.
[93] X. Guo, Y. Zhou, M. Yang, et al., “Research on control scheme for single converter online entry/exit in dual-converter based VSC-HVDC,” *Power Syst. Technol.*, vol. 43, no. 9, pp. 3393–3398, 2019.
[94] H. Xie, C. Fu, S. Li, et al., “Analysis on System Stability Characteristic of DC Line Fault Recovery and Converter Station Online Disconnection of KLL MTDC,” *Southern Power Syst. Technol.*, vol. 15, no. 6, pp. 7–14, 2021.
[95] C. Fu, J. Qiu, S. Li, et al., “Stability control strategy and system design for Kunliulong multi-terminal HVDC transmission,” *Southern Power Syst. Technol.*, vol. 16, no. 1, pp. 33–40, 2022.
[96] H. Xie, G. Peng, T. Yao, et al., “Analysis and optimization measures of anomaly valve-controlled trigger in Kunliulong hybrid multi-terminal UHVDC project,” *Southern Power Syst. Technol*., vol. 18, no. 3, pp. 104–110, 2024.
[97] I. Subotić, D. Gross, “Energy-balancing dual-port grid-forming control for VSC-HVDC systems,” *IFAC-PapersOnLine*, vol. 56, no. 2, pp. 6447–6452, 2023.
[98] I. Subotić, D. Groß, “Universal dual-port grid-forming control: bridging the gap between grid-forming and grid-following control,” *IEEE Trans. Power Syst.*, 2024.
[99] R. Yang, G. Shi, C. Zhang, et al., “Internal energy based grid-forming control for MMC-HVDC systems with wind farm integration,” *IEEE Trans. Ind. Appl.*, vol. 59, no. 1, pp. 503–512, 2022.
[100] D. Groß, E. Sánchez-Sánchez, E. Prieto-Araujo, et al., “Dual-port grid-forming control of MMCs and its applications to grids of grids,” *IEEE Trans. Power Del.*, vol. 37, no. 6, pp. 4721–4735, 2022.
[101] H. Zhang, W. Xiang, J. Wen, “Dual grid-forming control with energy regulation capability of MMC-HVDC system integrating offshore wind farms and weak grids,” *IEEE Trans. Power Syst.*, vol. 39, no. 1, pp. 261–272, 2024.
[102] H. Kim, J. Kang, J. W. Shim, et al., “Exploiting redundant energy of MMC–HVDC to enhance frequency response of low inertia AC grid,” *IEEE Access*, vol. 7, pp. 138485–138494, 2019.
[103] S. Yang, J. Fang, Y. Tang, et al., “Modular multilevel converter synthetic inertia-based frequency support for medium-voltage microgrids,” *IEEE Trans. Ind. Electron*., vol. 66, no. 11, pp. 8992–9002, 2019.

Haobo Zhang received his B.Eng. and PhD degrees both in electrical engineering from Huazhong University of Science and Technology (HUST), China in 2020 and 2025 respectively. He was a visiting PhD student at the Nanyang Technological University (NTU) from 2023 to 2024. Currently, he is a Research Associate at Cardiff University, UK. His research interests include protection and control of MMC-HVDC and DC grids.

Jinyu Wen (M’10-SM’25) received his B.Eng. and Ph.D. degrees all in electrical engineering from Huazhong University of Science and Technology (HUST), Wuhan, China, in 1992 and 1998, respectively. He was a visiting student from 1996 to 1997 and research fellow from 2002 to 2003 all at the University of Liverpool, UK, and a senior visiting researcher at the University of Texas at Arlington, USA in 2010. From 1998 to 2002 he was a director engineer in XJ Electric Co. Ltd. in China. In 2003 he joined the HUST and now is a Professor at HUST. His current research interests include renewable energy integration, energy storage application, DC grid, and power system operation and control.

Wang Xiang (S'16-M'17-SM'25) received his B.Eng. and PhD degrees both in electrical engineering from Huazhong University of Science and Technology (HUST), China in 2012 and 2017 respectively. He was a visiting PhD student at the University of Aberdeen and the University of Strathclyde in 2014 and 2016 respectively. He was with the University of Strathclyde from 2018 to 2021. Currently, he is a Professor at School of Electrical and Electronics Engineering, Huazhong University of Science and Technology, China. His main research interests include MMC-HVDC, high power DC/DC converters, DC grids and offshore wind power integration.

Weixing Lin received the B.E. and Ph.D. degrees in electrical engineering from the Huazhong University of Science and Technology, Wuhan, China, in 2008 and 2014, respectively. His research interests include HVDC, MMC, DC-DC autotransformer, and DC grids.

Meng Zhou received the Ph.D. degree in electrical engineering from the School of Electrical and Electronic Engineering, Huazhong University of Science and Technology (HUST), Wuhan, China, in 2019. He is currently a Postdoctoral Researcher with the School of Electrical and Electronic Engineering, HUST. His research interests include voltage-source converter-HVDC and DC circuit breaker.

Wenping Zuo received the B.S. degree and Ph.D. degree in electrical engineering from the Huazhong University of Science and Technology (HUST), Wuhan, China, in 2009 and 2017, respectively. He is currently a Postdoctoral Research Fellow with HUST. His research interests include DC grid key equipment, energy storage, and renewable energy integration.

Shijie Cheng (Life Fellow, IEEE) received the B.S. degree in electrical engineering from Xi'an Jiaotong University, Xi'an, China, in 1967, the M.Sc. degree in electrical engineering from the Huazhong University of Science and Technology (HUST), Wuhan, China, in 1981, and the Ph.D. degree in electrical engineering from the University of Calgary, Calgary, AB, Canada, in 1986. He has been a Professor with the School of Electrical and Electronics Engineering, HUST, since 1991. His research interests power system control, stability analysis, application of artificial intelligence, and energy storage. Prof. Cheng is a Fellow of the Chinese Academy of Sciences, Beijing, China.